3D Reconstruction and Visualization of Spiral Galaxies

Kristian Hildebrand

MPI Informatik
Stuhlsatzenhausweg 85
Saarbrücken, Germany
khildeb@mpi-inf.mpg.de

Marcus Magnor

Technical University of Braunschweig
Muehlenpfordtstrasse 23
Braunschweig, Germany
magnor@mpi-inf.mpg.de

Bernd Fröhlich

Bauhaus University Weimar
Bauhausstrasse 11
Weimar, Germany
bernd.froehlich@medien.uni-weimar.de

ABSTRACT

Spiral Galaxies are among the most stunning objects in the night sky. However, reconstructing a 3D volumetric model of these astronomical objects from conventional 2D images is a hard problem, since we are restricted to our terrestrial point of view. This work consists of two contributions. First, we employ a physically motivated, GPU-based volume rendering algorithm which models the complex interplay of scattering and extinction of light in interstellar space. Making use of general galactic shape information and far-infrared data, we secondly present a new approach to recover 3D volumes of spiral galaxies from conventional 2D images. We achieve this by an analysis-by-synthesis optimization using our rendering algorithm to minimize the difference between the rendition of the reconstructed volume and the input galaxy image. The presented approach yields a plausible volumetric structure of spiral galaxies which is suitable for creating 3D visualization, e.g., for planetarium shows or other educational purposes.

Keywords
3D visualization, astronomical visualization, 3D reconstruction

1 Introduction

The night sky emanates a deep fascination. It has been the target of contemplation and research efforts since the earliest beginnings of human culture. The colorful, attractive appearance of astronomical objects is awe-inspiring. Besides their esthetical value, astrophysicists are able to draw conclusions about the origin of the cosmos from scientifically studying these objects. Therefore, telescopes around the world and in space record and collect data that is not only useful for physicists but also stunning and beautiful to everybody on earth.

By looking through an eye-piece of a telescope one can see various objects in the night sky, e.g. planets, stars, all sorts of nebulae and galaxies. To get an impression on how these objects look like from a different viewpoint than our terrestrial position one has to visualize astronomical objects in their three-dimensional shape and simulate the visual effects by exploring physical properties of light in interstellar material.

The increasing interest of 3D visualization in TV documentaries, science fiction movies, games and education makes it desirable to find a realistic representation of astronomical objects. Todays animations are often based on a more artistic then physically correct representation of astronomical objects, even though it is useful to give a more realistic impression of what can be observed. Furthermore we can use our results to provide additional information in telescope applications like recently published by Linţu et al. [LM05] to increase the understanding of the observed data.

In this paper we present an approach on how to determine the three-dimensional shape of *spiral galaxies* from conventional 2D images, which is, in general, a very challenging problem, due to our restricted point of view.

However, our approach relies on several physical information about the object, like a general shape evolved from its formation. Additionally we use different band-filtered data from the objects observation to gain more insights of the material it consists of. The appearance of *spiral galaxies* is significantly determined
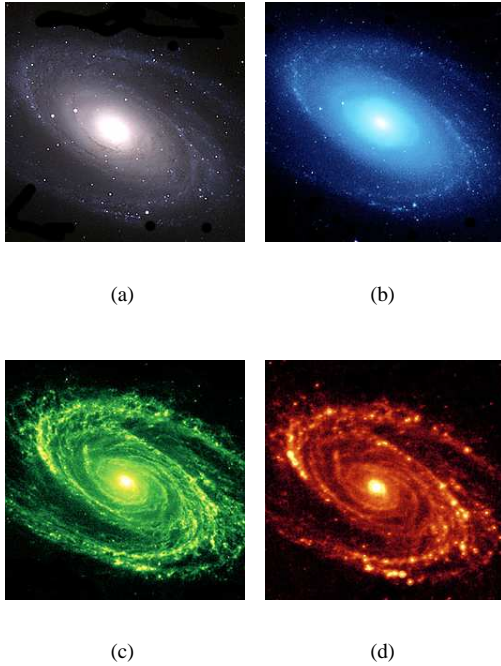
Figure 1: M81 as photographed from the Spitzer Space Telescope in the infrared light ©NASA/Spitzer [Tel]. (a) Galaxy M81 in visible light. (b), (c), (d) M81 at three different infrared wavelengths (3.6, 8, and 24 μm, respectively).

by the amount of interstellar material within the galaxies, because clouds of dust have scattering and extinction properties at different visible-light wavelengths as can be seen in Figure 4 from [BM98]. To be able to reconstruct a 3D volumetric model of *spiral galaxies* we have to simulate these effects.

The paper is structured as follows. After a brief overview of related work, we provide some fundamental background information about galaxies in Section 3 We describe our volumetric radiance model, which is important for the reconstruction process in Section 4 and illustrate in detail how to recover the actual 3D volumetric shape in Section 5 Our results are presented in Section 7

2 Previous Work

Pioneering work in visualizing virtual space journeys was done by Jim Blinn [Bli87] and his set of animations called 'Voyager Fly-by Animations', 'Cosmos' and 'The Mechanical Universe' from the late 70ies and early 80ies. Many spectacular, almost always artistic, 3D fly-throughs of astronomical objects can be seen in planetariums. An exceptionally physically based work is done by Nadeau et al. [NGN+01], [NE]. They employed massive computational power to create scientifically justified views of the orion nebula. Their vi-

sualization relies on a 3D model of the Orion nebula that was determined by astronomers from various observational data [ZO95]. Hanson et al. [HFW00] did a lot of work on large scale visualization of astronomical data and more recently on exploring the physical Universe as an enormous environment. They introduce a so-called powers-of-ten visualization architecture to provide scale-independent modeling and rendering [FH05].

Magnor et al. [MKH04] recently reconstructed and rendered 3D models of planetary nebulae. Former astrophysical research had shown that some planetary nebulae have specific symmetry characteristics due to physical processes of their formation. The basic idea is to use astronomical image data and symmetric structural constraints of the nebulae to reconstruct the three-dimensional volume by an analysis-by-synthesis approach. They introduced the term *constraint inverse volumetric rendering* (CIVR) as a GPU-based optimization procedure to reconstruct a volumetric model for planetary nebulae. Magnor et al. [MHLH05] most recently visualized physically correct *reflection nebulae* by taking into account the astrophysical properties of dust in interstellar space. *Reflection nebulae* are clouds of interstellar dust which are reflecting visible light of a nearby star or stars. That results in a very colorful interplay between scattering and extinction effects and makes them one of the most colorful objects in the night sky. The used volume rendering approach employs the Henyey-Greenstein scattering phase function to create a lookup table for the amount of light scattered in the observer's direction [HG41], [Gor04], [HG38]. The synthetic data sets mimic artificially generated reflection nebulae very realistically.

In this paper we rely on the proposed reconstruction and rendering technique ([MKH04], [MHLH05]) but employ different optimization constraints and an adopted visualization model.

Fundamental basic knowledge and research about galactic astronomy can be found in Binney et al. [BM98]. They provide a complete overview of colors, morphology and photometry of galaxies, as well as the properties of interstellar material and its effect on observed data.

3 Background

A galaxy is a system of stars, interstellar gas and dust, dark matter in the center and possibly dark energy. Galaxies usually contain 10 million to one trillion stars orbiting a center of gravity. It consists of rarefied interstellar material, star clusters, single stars and various types of nebulae, such as emission-, dark-, planetary- and reflection nebulae. The generic shape in Figure 3 can be divided into a center bulge embedding very old stars, a circular disk of younger stars and a surround-

ing spherical halo [BM98].

3.1 Shape Classification

Astronomers classify galaxies based on their overall shape and further by the specific properties of the individual galaxy, like the number of spiral arms, the degree of the ellipse or the pitch angle of the spiral. The system of galaxy classification is known as the Hubble sequence or Hubble tuning fork which is shown in Figure 2. This classification scheme starts at the left with *elliptical galaxies* (E0-E6 types) divided by the factor of oval-shape. Then the diagram splits into two branches. The upper branch shows *spiral galaxies* (Sa-Sc types) which are basically split into different spiral pitch angles. The lower branch (SBa-SBc types) covers *barred-spiral galaxies* that differ in their characteristic formed bar in contrast to the spherical shaped bulge of Sa-Sc types. We will focus on recovering galaxies of type Sb and Sc using data from the Spitzer telescope [Tel], in particular Galaxy M81, a publicly available data set that can be used for the proposed reconstruction method.
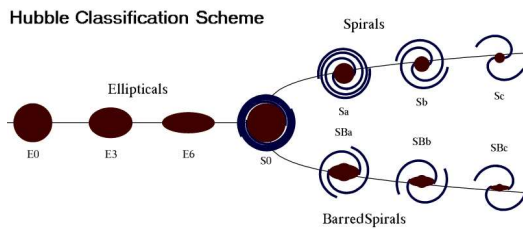

Figure 2: Hubble Classification Scheme ©S.D. Cohen (from [Coh]). The Hubble Classification Scheme is able to capture the topological diversity of most galaxies. From left to right, spherical and elliptical shapes are succeeded by spirals of different extent, with or without a central bar.

The arms of spiral galaxies approximately have the shape of a logarithmic spiral and are areas of high density or density waves and can be observed at visible wavelengths. The high concentration of gas and dust in the arms facilitates star formation of very bright stars.

3.2 Interstellar Dust

A galaxy viewed from the front, the so-called face-on view, shows dark spiral stripes containing interstellar dust (see Figure 3). Interstellar dust has the property to scatter and absorb photons at different wavelength. Blue light is scattered more often, because the size of many of the individual grains of space dust is about the same as the wavelength for blue light varying between $100nm$ and $1\mu m$. It means, that much

of the blue light emitted from stars in the galaxy behind the dust clouds gets scattered away from our direct view, making the stars in the galaxy, as we see them through the dust look redder and dimmer than they actually are [BM98]. The wavelength-dependent scattering properties of particles are described by the Mie scattering theory [vdH82]. Furthermore photons that get absorbed from the dust convert the energy into heat. Thus, the dust transforms blue light into far infrared light and the absorption of starlight warms dust grains to $\approx 10K$. At this temperature they radiate significantly at $\lambda \approx 200\mu m$, and photons of this wavelength can escape.

Figure 1 shows infrared images obtained by Spitzer's infrared array camera, a space telescope to obtain images and spectra in infrared at wavelengths between 3 to 180 micron, that cannot be detected from Earth [Tel]. It exhibits a four-color composite of Galaxy M81 which is located at a distance of 12 million light-years from Earth. The images of visible and invisible light show emissions from wavelengths of 3.6 microns (blue), 8 microns (green), and 24.0 microns (red). Images in near-infrared collected at 3.6 micron trace the distribution of older and redder stars and are virtually unaffected by obscuring dust. As one moves to longer wavelengths, the spiral arms become the dominant feature of the galaxy. The 8 micron emission is dominanted by infrared light radiated by hot dust that has been heated by nearby luminous stars. The dust particles are composed of silicates, carbonaceous grains and polycyclic aromatic hydrocarbons and trace the gas distribution in the galaxy. The well mixed gas and dust, which is best detected at radio wavelengths, provide a reservoir of raw materials for future star formation. The 24-micron image shows emission of warm dust heated by the most luminous young stars. The bright knots show where massive stars are being born. These star formation regions are of great astrophysical interest because they help identifying the conditions and processes of star formation [Tel].
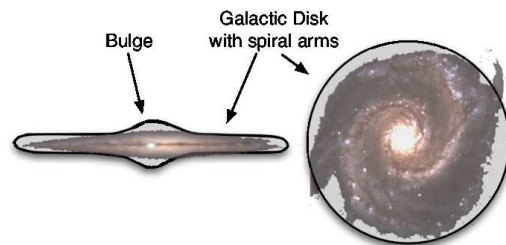

Figure 3: Generic Galaxy Shape. On the left is the so-called edge-on view (90°). The dust is concentrated along a galaxy's equatorial region. Compared to the right, which is often referred to as face-on view (0°), where the dust is concentrated along the spiral arms.

4 Galaxy Visualization

From our terrestrially confined viewpoint, recovering the actual three-dimensional shape of distant astronomical objects is very challenging. The key to reconstruct a 3D *spiral galaxy volume* from an 2D image is to find a visualization technique which is able to reproduce the visual effects of the galaxies appearance. Figure 4 shows that due to the distribution of dust within the galaxy a complex interplay of light and dust takes place. The appearance of galaxies as we see them can be described by effects of scattering and extinction [BM98]. Thus, we need to find a visualization model that simulates realistically these effects.
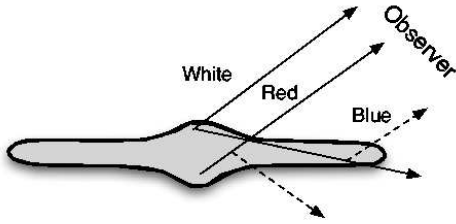

Figure 4: Effects of scattering and absorption of light by dust. Light from the top reaches the observer without obstruction. Light from the lower part is partially absorbed and scattered into the path of the observer.

4.1 Volumetric Radiance Model

At this point we can make use of a method proposed by Magnor et al. [MHLH05]. They are simulating the effects of interstellar dust for *reflection nebulae*. Adopting their visualization model to galaxies can be done as follows: first, we subdivide the space around the galaxy into voxels. Each voxel is assigned the radiance L_{ill} arrived at the voxel from the stars and a value proportional to the density of dust π_{sct}, where $\pi_{sct} = \sigma_{sct} \cdot l$, with l as the size of the voxel and σ_{sct} as the scattering coefficient, the average amount of scattering, for a voxel.

Only a fraction $P(\pi_{sct})$ of the radiance L_{ill} at a voxel is scattered into the observers direction to define L_{sct}. $P(\pi_{sct})$ is pre-computed and tabulated using a Monte-Carlo simulation. Since we assume isotropic scattering due to the large-scale structure, the portion of scattered light is not direction-dependent in contrast to reflection nebulae rendering [MHLH05].

$$L_{sct} = L_{ill} \cdot P(\pi_{sct}) \qquad (1)$$

However, the scattered light still must travel the path form the voxel to the observer, where it also is attenuated along the line of sight due to optical depth $\pi_{opt} = \pi_{sct}/a$ in the interstellar medium. The albedo, $a = [0, 1]$ can be described as the average percentage of radiation that is being scattered on a single dust

particle. It becomes zero when the dust is completely black and all incident radiation is absorbed and one when all photons are deflected by the particle. As pointed out in [Gor04], it is reasonable to assume that for the current measured and analyzed data at visible wavelengths the albedo is $a \approx 0.6$ throughout the galaxies. That yields

$$L = L_{sct} \cdot exp^{-\int_0^l \pi_{opt}(l')dl'}. \qquad (2)$$

Since π_{sct} and π_{opt} vary with wavelength we compute L separately for the red, green and blue channel. Binney et al. [BM98], Magnor et al. [MHLH05] and Cardelli et al. [CCM89] illustrate the wavelength-dependent effects of extinction which can be described by astrophysical parameters such as the *ratio of total-to-selective extinction*. We also take these values into account.
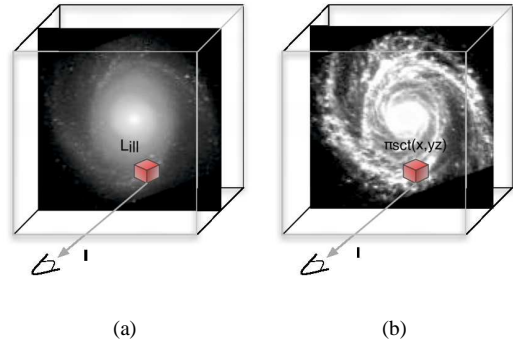

(a)   (b)

Figure 5: Discretization of the space around the galaxy into voxels. Each voxel emits light according to local star density (a). A fraction of the light is scattered depending on dust density or scattering depth π_{sct}. More light is absorbed on distance l from the voxel to the observer.

Figure 5(a) shows the radiance L_{ill} that is received at a volume position (x,y,z) and the scattering depth π_{sct} proportional to the dust density in Figure 5(b) . More details on how we can derive these values from the 2D observations for reconstruction are described in Section 5

4.2 Interactive GPU-Raycasting

Our rendering algorithm relies on graphics hardware-based ray-casting. The basic idea, proposed by Krueger [KW03], is simple. The dataset is stored in a 3D texture to take advantage of built-in trilinear filtering. Then a bounding box geometry is created encoding the position in the data set as colors, i.e., we can interpret these as 3D texture coordinates.

The rendering algorithm runs in four passes. The first two passes prepare the proxy-geometry, i.e., render

front- and back-faces, and compute the ray direction and length. In the third pass we first issue a fragment program to step along the viewing vector from front to back in voxel length intervals. The pre-computed scattering table $P(\pi_{sct})$ is uploaded as a 1D floating-point texture to graphics memory. A 3D floating point texture stores scattering depth π_{sct} and illumination L_{ill} for each voxel. At each step along the ray we lookup local scattering depth π_{sct} and voxel illumination L_{ill} from the 3D volume textures. These values are trilinear interpolated on graphics hardware. Then the fragment program queries the scattering lookup table to determine $P(\pi_{sct})$. L_{sct} can be determined by (1). L_{sct} undergoes extinction $\sigma_{ext} = \pi_{sct}/a$ on the line of sight which is accumulated by stepping along the ray to compute L (2). The image correction is done in the final fourth pass.

5   3D Reconstruction

The proposed visualization model is able to capture the general effects of interstellar material that are responsible for the overall appearance of galaxies. However, to reconstruct the galaxy from a conventional 2D image we have to recover dust density and light distribution information from observational data.

Before analyzing the images in Figure 1 we compute their geometric moments up to the second order and center, rotate and de-project the images, i.e., correct to a face-on view as commonly done in astrophysical research. Now, we can recover approximately the density of dust by adding up Figure 1(c) and Figure 1(d). Adding up the dust images is essentially like accumulating different sorts of interstellar material that radiate at different infrared wavelengths because of their size and temperature. The image intensity can be then interpreted as a dust density which is proportional to the scattering depth π_{sct}, shown in Figure 6(b). The radiance L_{ill} received at a voxel can be taken from Figure 6(c) which shows the star light unaffected by obscuring dust and can be interpreted as the distribution of light at a specific point in the galaxy.

However, we still have to take the amount of light into account that gets scattered in the observer's direction. Also, we account for the attenuation by optical depth when light travels through the galaxy to the observer as seen in Eq. (1) and (2). L_{ill} and π_{sct}, taken from the observational data, are sufficient to define our volume data structure.

We now can try to fit our 2D image in the generic galaxy shape using a simple back-projection approach. By back-projecting the image we smear it through the volume constraint by the generic galaxy shape which can be described by a gaussian function (see Figure 3). We discard all values outside the model and weight their contribution according to the distance from the

(a)   (b)

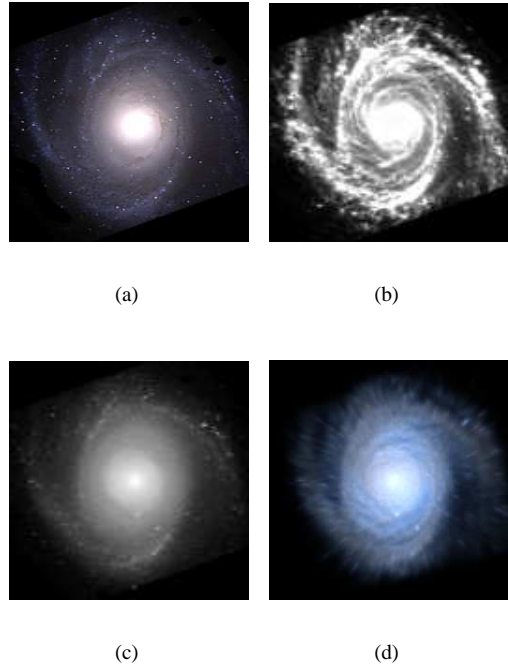(c)   (d)

Figure 6: Reconstruction results from infrared image data, see Figure 1. We can achieve similar rendering results by extracting a dust distribution from the infrared images. (a) Original image in visible light, deprojected to face-on view. (b) Reconstructed dust distribution (c) Star light distribution at $3.6\mu m$ (d) Resulting rendition.

center.

However, just back-projecting the dust distribution into the generic shape creates stripes that make the image look unnatural. Using procedural noise [Per85] we can break up these stripes in a more natural way.

Figure 6 shows, that the original image (a) can be implicitly reconstructed by using the dust distribution (b) and a radiance profile in image (c). Image (d) shows the result. It is interesting to see that without any further information, just by using dust and light distribution we can achieve a similar appearance of the galaxy. The blueish tint of the rendition (d) shows the assumed dust density map is not sufficient enough to reconstruct the galaxy realistically.

Using the adopted *reflection nebulae* rendering [MHLH05], [Hil05] is still an approximation, since the effects of scattering and absorption effects for the nebulae are only evaluated locally for a few stars and not globally for the entire galaxy. However, we can assume a dust density or scattering depth π_{sct} and a radiant power of star light L_{ill} at any voxel for our galaxy visualization model. By reconstructing a dust density map from several band-filtered infrared images it is possible to find a valid representation for an original image. As mentioned in Section 3.2 mid- and far-

infrared data provide necessary information about the dust distribution of the galaxy. Now, we can expand this approach by using the reconstructed dust density map as an initialization parameter for an analysis-by-synthesis algorithm to approximate the original shape more closely.

6 Analysis-by-Synthesis Reconstruction

3D image analysis-by-synthesis is the general concept of inverting the image formation process by solving the forward problem repeatedly while adjusting the parameters of the reconstruction until the differences between the original and the synthesized image are minimized.
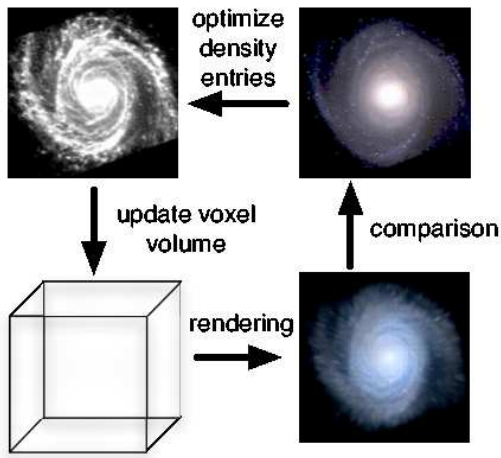

Figure 7: Analysis-by-synthesis scheme for spiral galaxy reconstruction. The volume is rendered and the difference between rendition and original is evaluated using sum-of-squared differences. After optimizing the model parameters in the dust density distribution we update the volume and render again.

The *spiral galaxy* reconstruction approach relies on constraint inverse volume rendering (CIVR), Magnor et al. [MKH04]. However, our CIVR approach is based on the generic shape of the galaxy and the proposed visualization method. The model we want to optimize is the dust density map which is proportional with the scattering depth π_{sct}. The approximated image in Figure 6(b) can be used as prior knowledge and as an initial guess for the optimization. The galaxy rendering provides the basis of our approach, since we assume that it is a plausible way to realistically visualize galaxy volumes. It is important to understand that a visualization which cannot provide plausible renderings, cannot be used for this approach, since we rely on evaluating the error functional based on the rendition and the image difference.

Given that the galaxy visualization is a non-linear process we employ non-linear optimization, i.e., a standard implementation of Powell's non-linear optimization method [PFTV92]. *Powell's direction set* numerically evaluates the error function's local slope along all dimensions of the model $m_{1...N}$ from which it determines the *conjugate-gradient* direction.

The aim of the optimization is to determine the closest possible solution for the 2D projection, i.e., the volume rendering result that matches as closely as possible with the original galaxy image at visible wavelengths. Each optimization iteration step entails a modification in the volume data set, uploading the modified data onto the graphics card, rendering the model again and re-evaluating the error measure, as shown in Figure 7. To qualify the difference between both images we compare the corresponding pixel using the sum-of-squared-differences (SSD)

$$\arg \min_{d_{1...N}} \sum (p(x,y) - p_r(x,y))^2 \qquad (3)$$

where $d_{1...N}$ denotes the parameters in the dust density map and the color parameters for the overall approximated star colors. Additionally, the error functional penalizes negative values and scattering depth π_{sct} values that reach outside the scattering table for values $\pi_{sct} > 10.0$. The color values are also penalized, if they fall outside the RGB range. That allows us to constrain our optimization to physically reasonable values. Magnor et al. [MKH04] employed several error functionals of which the SSD error measure yielded the fastest convergence. The algorithm table summarizes the steps again:

Algorithm 1 Analysis-by-Synthesis

    Back-project illumination and dust density map into generic shape;
    Render galaxy volume;
    Initialize optimization parameters, i.e., 2D scattering depth;
    while Convergence not reached **do**
        Render volume;
        Optimization using Powell's Direction Set;
        Compute SSD to evaluate error;
        Penalize parameters that are out of range;
        Update optimization parameters, i.e., 2D scattering depth and color values;
        Back-project and update 3D volume on the graphics card;
    end while

The algorithm stops, when the difference between optimization steps is lower than a certain tolerance value. From the optimization point of view this approach underlies a high-dimensional parameter space. Each iteration step we modify our parameters until the algo-

rithm converges to a minimum of the error function. Since we are dealing with a non-linear optimization problem, a global convergence to the global minimum can not be guaranteed.

If the initial guess is not close to the global minimum, or the parameters are not reasonable constraint, the algorithm does not converge to a physically plausible solution. Also, if our rendering procedure does not map the values closely to the original projection a convergence cannot be expected, because we are not able to produce the desired values.
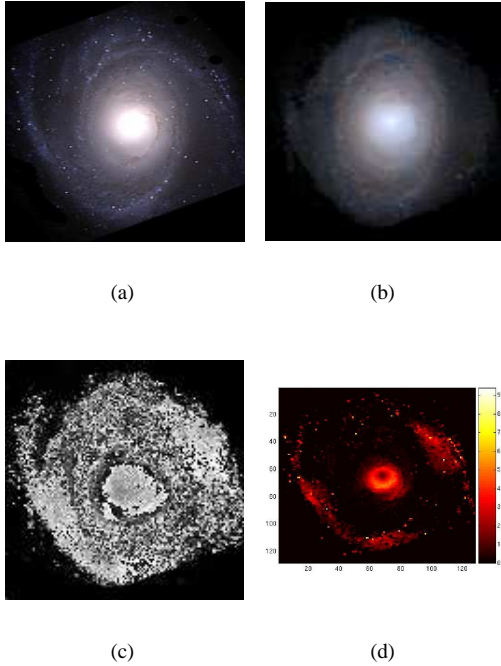

| (a) | (b) |

| (c) | (d) |

Figure 8: Figure (a) shows the original M81 image deprojected to face-on view. (b) M81 after analysis-by-synthesis optimization. (c) Reconstructed dust density map.(scaled for displaying purposes) (d) Difference image between original and optimized image.

7   Results

Figure 8 shows that the reconstructed image (b) closely resembles the original galaxy photograph (a). The proposed visualization model is able to recover the overall appearance of galaxies. The dust density distribution entries are optimized which is a sufficient model to reconstruct the volume. Despite a reasonable guess for our analysis-by-synthesis procedure the optimization computation took about three days on a 3.0Ghz Pentium4 with nVidia GeForce 6800 Ultra graphics board. Figure 8(d) shows the difference between original and reconstruction. One can see that especially the galactic bulge area exhibits high differences. That is because the dust consistency changes drastically throughout the galaxy center due to very hot stars. The reconstructed dust density distribution varies compared to initial guess in Figure 6(b) and is very noisy. The reason is that there are many regions where dust density changes, e.g. because of star formation.
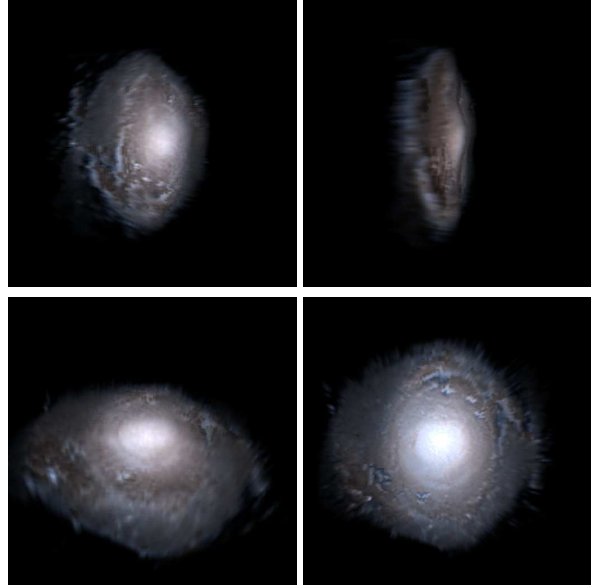

Figure 9: Resulting fly-by images for the presented 3D volume reconstruction of Spiral Galaxy M81.

Figure 9 shows that the proposed method recovers an approximated, plausible shape of the volume using the galaxy rendering, which yields the conclusion, that the proposed method is a promising approach to attack the problem.

However, there are still a lot of problems, mostly related to approximations in the visualization model. The radiance map, as seen in Figure 6(c), doesn't have enough influence on the rendering to display the bluish areas along the spiral arms. That should be taken into account during optimization. Furthermore, we should take other physical parameters into account to represent the galaxies appearance more closely.

8   Conclusion

We have presented an adopted rendering method to reconstruct a plausible shape for *spiral galaxy M81*. Its inherent generic shape and additional observations in far-infrared enable us to use a model to describe the galaxy's three-dimensional dust distribution in space, thereby constraining the reconstruction problem. By rendering realistic images of our model and comparing the rendering results to the original image data, we employ an optimization approach that helps converge towards a reasonable dust density distribution for the galaxy. Using the optimized model we are able to closely resemble a realistic appearance of the galaxy

by fitting the values to a generic shape. Figure 9 shows a series of images from different view points around galaxy M81.

References

[Bli87]   J. Blinn. Voyager fly-by animations. *Animations depicting space missions to Jupiter, Saturn and Uranus*, 1977-87.

[BM98]   J. Binney and M.Merrifield. Galactic astronomy. *Princeton University Press*, 1998.

[CCM89]   J. Cardelli, G. Clayton, and J. Mathis. The relationship between infrared, optical and ultraviolet extinction. *Astrophysical Journal*, pages 345:245–256, 1989.

[Coh]   S. D. Cohen. Hubble classification scheme. *website:* `http://en.wikipedia.org/wiki/Image:Hubblescheme.png`. *visited August 2005.*

[FH05]   Chi-Wing Fu and A. Hanson. The powers-often visualization architecture for exploring the physical universe. *submitted for publication*, 2005.

[Gor04]   K. Gordon. Interstellar dust scattering properties. in a. witt, g. clayton, and b. draine, editors. *Astrophysics of Dust. ASP conference series*, 2004.

[HFW00]   A.J. Hanson, Chi-Wing Fu, and E.A. Wernert. Very large scale visualization methods for astrophysical data. *Proceedings of the Joint Eurographics and IEEE TVCG Symposium on Visualization*, pages 115–124, 2000.

[HG38]   J. Henyey and J. Greenstein. The theory of the colors of reflection nebulae. *Astrophysical Journal*, 88:580–604, 1938.

[HG41]   J. Henyey and J. Greenstein. Diffuse radiation in the galaxy. *Astrophysical Journal*, 93:70–83, 1941.

[Hil05]   K. Hildebrand. Rendering and reconstruction of astronomical objects. *Diploma Thesis*, 2005.

[KW03]   J. Krueger and R. Westermann. Acceleration technique for gpu-based volume rendering. *Proceedings of IEEE Visualization*, pages 287–292, 2003.

[LM05]   A. Lințu and M. Magnor. Augmented astronomical telescope. *Second GI-Workshop VR/AR Proceedings*, 2005.

[MHLH05]   M. Magnor, K. Hildebrand, A. Lințu, and A. Hanson. Reflection nebula visualization. *Proc. IEEE Visualization*, pages 255–262, 2005.

[MKH04]   M. Magnor, G. Kindlmann, and H. Hansen. Constrained inverse volume rendering for planetary nebulae. *Proceedings of IEEE Visualization*, pages 83–90, 2004.

[NE]   D. Nadeau and E. Engquist. Volume visualization of the evolution of an emission nebula. *website:* `http://vis.sdsc.edu/research/hayden2.html`. *visited January 2005.*

[NGN+01]   D. Nadeau, J. Genetti, S. Napear, B. Pailthrope, C. Emmart, E. Wesselak, and D. Davidson. Visualizing stars and emission nebulae. *Computer Graphics Forum*, 20:27–33, 2001.

[Per85]   K. Perlin. An image synthesizer. *Proceedings of ACM SIGGRAPH*, pages 287–296, 1985.

[PFTV92]   W. Press, B. Flannery, S. Teukolsky, and W. Vetterling. Numerical recipes in c. *Cambridge University Press*, 1992.

[Tel]   Spitzer Space Telescope. *website:* `http://www.spitzer.caltech.edu/`. *visited June 2005.*

[vdH82]   H. van de Hulst. Light scattering by small particles. *Dover Publications Inc., New York*, 1982.

[ZO95]   W. Zhen and C. ODell. A three-dimensional model of the orion nebula. *Astrophysical Journal*, 438:784–793, 1995.